

Synthesis and characterization of the first tin fluoride borate $\text{Sn}_3[\text{B}_3\text{O}_7]\text{F}$ with second harmonic generation response

Sandra Schöneegger, Stephan G. Jantz, Andreas Saxer, Lkhamsuren Bayarjargal, Björn Winkler, Florian Pielhofer, Henning A. Höpfe, Hubert Huppertz

Angaben zur Veröffentlichung / Publication details:

Schöneegger, Sandra, Stephan G. Jantz, Andreas Saxer, Lkhamsuren Bayarjargal, Björn Winkler, Florian Pielhofer, Henning A. Höpfe, and Hubert Huppertz. 2018. "Synthesis and characterization of the first tin fluoride borate $\text{Sn}_3[\text{B}_3\text{O}_7]\text{F}$ with second harmonic generation response." *Chemistry - A European Journal* 24 (60): 16036–43. <https://doi.org/10.1002/chem.201803478>.

Nonlinear optics | *Hot Paper*


 Sandra Schönegger,^[a] Stephan G. Jantz,^[e] Andreas Saxer,^[b] Lkhamsuren Bayarjargal,^[c] Björn Winkler,^[c] Florian Pielhofer,^[d] Henning A. Höpfe,^{*,[e]} and Hubert Huppertz^{*,[a]}

Abstract: The new non-centrosymmetric tin fluoride borate $\text{Sn}_3[\text{B}_3\text{O}_7]\text{F}$ was synthesized hydrothermally, and was characterized by single-crystal and powder X-ray diffraction, vibrational spectroscopy, DFT calculations, second harmonic generation (SHG) measurements, thermogravimetry, and differential scanning calorimetry. Its SHG response is about 12 times that of quartz. The compound crystallizes in the non-centrosymmetric orthorhombic space group $Pna2_1$ with lat-

tice parameters $a=922.4(2)$, $b=769.8(4)$, and $c=1221.9(6)$ pm ($Z=4$). Characteristic for the structure are isolated B_3O_7 moieties, consisting of two corner-sharing BO_3 units and one BO_4 tetrahedron. These occupy half of the octahedral voids of a slightly distorted hexagonal closest packing of Sn^{2+} atoms, with $[\text{SnF}]^+$ units in the other half of the octahedral voids. $\text{Sn}_3[\text{B}_3\text{O}_7]\text{F}$ is transparent over a wide spectral range with a UV cut-off edge at about 263 nm.

Introduction

At the beginning of the 1960s, shortly after the demonstration of the first laser, Franken et al.^[1] observed for the first time second harmonic generation (SHG) when illuminating a quartz crystal with a ruby laser. This has triggered the on-going search for non-linear optical (NLO) materials suitable for a very broad range of applications. However, the challenge remains

to obtain new NLO materials having a combination of desirable properties, such as large SHG coefficients, moderate birefringence, transparency over a broad spectral range for phase matching, a high damage threshold, good chemical stability, and facile crystal growth.^[2–4]

Borates are of great interest as NLO materials as the boron atom in borates possesses the ability to coordinate either three or four oxygen atoms to form trigonal planar $[\text{BO}_3]^{3-}$ or tetrahedral $[\text{BO}_4]^{5-}$ units. These building units within a chiral structure adopt a coplanar configuration to promote SHG and birefringence. A variety of NLO borates are already known, including $\beta\text{-BaB}_2\text{O}_4$ (BBO),^[5] LiB_3O_5 (LBO),^[6] CsB_3O_5 (CBO),^[7] $\text{CsLiB}_6\text{O}_{10}$ (CLBO),^[8,9] and $\text{YCa}_4\text{O}(\text{BO}_3)_3$ (YCOB).^[10] A breakthrough in the area of deep-UV NLO crystals was achieved with the discovery of $\text{KB}_2\text{BO}_3\text{F}_2$ (KBBF),^[11] because it is the only material that can produce coherent light by direct SHG at wavelengths below 200 nm. The distinctive crystal structure of KBBF results in excellent NLO properties, such as moderate SHG coefficients, a wide viewing window, and a good birefringence. Further fluoride borates include $\text{Pb}_3\text{B}_6\text{O}_{11}\text{F}_2$,^[12] $\text{Ba}_3\text{B}_6\text{O}_{11}\text{F}_2$,^[13] $\text{Cd}_5(\text{BO}_3)_3\text{F}$,^[14] and the fluorooxoborates $\text{BiB}_2\text{O}_4\text{F}$,^[15] $\text{NaB}_4\text{O}_6\text{F}$,^[16] $\text{SrB}_5\text{O}_7\text{F}_3$,^[17] $\text{CsB}_4\text{O}_6\text{F}$ ^[18] have been reported, which also show SHG. All these compounds were synthesized using high-temperature synthesis methods, with $\text{Pb}_3\text{B}_6\text{O}_{11}\text{F}_2$ being an exception as it was produced under hydrothermal conditions at 240 °C. Furthermore, the first fluorooxoborate $\text{Sn}[\text{B}_2\text{O}_3\text{F}_2]$ was also obtained recently.^[19] Compared to our fluoride borate, $\text{Sn}[\text{B}_2\text{O}_3\text{F}_2]$ represents a fluorooxoborate.

Our group has already succeeded in synthesizing new tin borates in the Sn-B-O-H system like $\text{Sn}_2\text{B}_3\text{O}_6(\text{OH})$ ^[20] and $\text{SnB}_8\text{O}_{11}(\text{OH})_4$.^[21] Guided by the idea to synthesize the first tin fluoride borate under hydrothermal conditions in the system Sn-B-O-F, we successfully obtained the novel compound $\text{Sn}_3[\text{B}_3\text{O}_7]\text{F}$.

[a] S. Schönegger, Prof. Dr. H. Huppertz
Institut für Allgemeine, Anorganische und Theoretische Chemie
Leopold-Franzens-Universität Innsbruck
Innrain 80–82, 6020 Innsbruck (Austria)
E-mail: hubert.huppertz@uibk.ac.at
Homepage: <http://www-c724.uibk.ac.at/aac/>

[b] Dr. A. Saxer
Institut für Konstruktion und Materialwissenschaften
Leopold-Franzens-Universität Innsbruck
Technikerstraße 13, 6020 Innsbruck (Austria)

[c] Dr. L. Bayarjargal, Prof. Dr. B. Winkler
Institut für Geowissenschaften
Universität Frankfurt
Altenhöferallee 1, 60438 Frankfurt/Main (Germany)

[d] F. Pielhofer
Institut für Anorganische Chemie,
Universität Regensburg
Universitätsstraße 31, 93053 Regensburg (Germany)

[e] S. G. Jantz, Prof. Dr. H. A. Höpfe
Institut für Physik, Universität Augsburg
Universitätsstr. 1, 86159 Augsburg (Germany)
E-mail: henning@ak-hoeppe.de
Homepage: <http://www.ak-hoeppe.de>

Supporting information and the ORCID identification number(s) for the author(s) of this article can be found under:
<https://doi.org/10.1002/chem.201803478>.

© 2018 The Authors. Published by Wiley-VCH Verlag GmbH & Co. KGaA. This is an open access article under the terms of the Creative Commons Attribution License, which permits use, distribution and reproduction in any medium, provided the original work is properly cited.

Results and Discussion

Crystal structure

The crystal structure of $\text{Sn}_3[\text{B}_3\text{O}_7]\text{F}$ contains B_3O_7 groups forming three membered rings. The fundamental building block (FBB) consists of two corner-sharing BO_3 triangles and one BO_4 tetrahedron, described as $\langle \square 2\Delta \rangle$ [22] with the triangle and the square as pictograms for the trigonal-planar $[\text{BO}_3]^{3-}$ and the tetrahedral $[\text{BO}_4]^{5-}$ group, respectively (see Figure 1, encircled in red). Interestingly, the tips of the BO_3 groups are oriented once to the right (upper three membered rings) and once to the left (lower three membered rings). The $\text{Sn}1$ and $\text{Sn}3$ cations form a slightly distorted hexagonal closest packing with the three membered rings $\langle \square 2\Delta \rangle$ in one half of the octahedral voids; the other half of the octahedral voids are filled with $[\text{SnF}]^+$, as illustrated in Figure 2 and Figure S4 (Supporting Information). All these non-centrosymmetric $\langle \square 2\Delta \rangle$ rings are oriented in the same manner, resulting in a polar crystal structure along the c axis.

In the crystal structure of $\text{Sn}_3[\text{B}_3\text{O}_7]\text{F}$, there are three unique boron atoms. The boron atom B2 is tetrahedrally coordinated

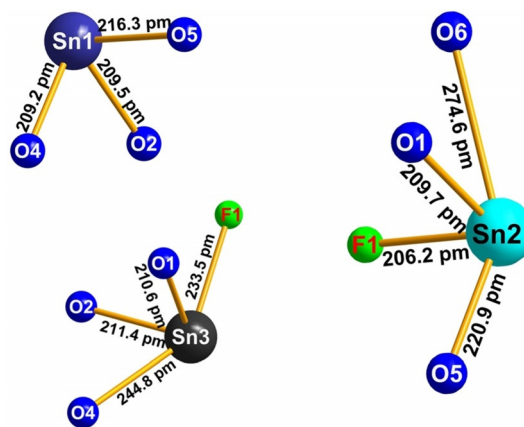


Figure 2. The three Sn^{2+} cations in $\text{Sn}_3[\text{B}_3\text{O}_7]\text{F}$ with the interatomic distances.

by four oxygen atoms. The B–O distances in the tetrahedron range between 145.9(5)–148.8(5) pm, in good agreement with the average value of 147.6 pm.^[22,23] The O–B–O bond angles in the $[\text{BO}_4]^{5-}$ group exhibit an average value of 109.5° , indistinguishable within error from the ideal tetrahedral angle of

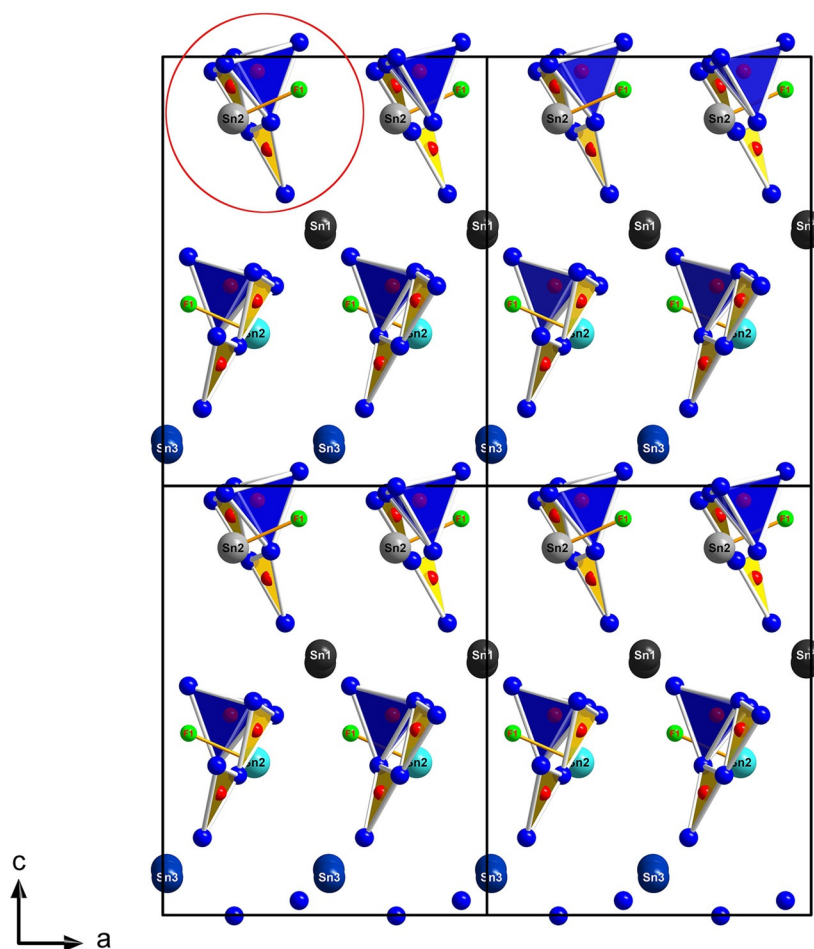


Figure 1. 2×2 unit cell along the b axis in the crystal structure of $\text{Sn}_3[\text{B}_3\text{O}_7]\text{F}$. The three-membered ring $\langle \square 2\Delta \rangle$ forming the fundamental building block (FBB) encircled in red. O^{2-} : small blue spheres; F^- : green spheres, B^{3+} : small red spheres, and the three Sn^{2+} cations: dark blue, dark grey and light blue. BO_4 groups are indicated with blue polyhedra and the BO_3 groups with yellow triangles.

109.47°. The atoms B1 and B3 are threefold coordinated by oxygen atoms forming BO_3 groups. The values of the O–B–O bond angles range from 117.1(4) to 122.3(4)° (mean value = 120.0°) and the B–O distances from 135.1(5) to 138.4(3) pm with an average value of 136.7 pm. This value agrees very well with the mean B–O distance of 137 pm for this coordination.^[22] Furthermore, there are three crystallographically unique Sn atoms, which possess different coordination environments (see Figure 2). The Sn1 cation coordinates three oxygen atoms, O2, O4, and O5 with Sn–O distances of 209.0(3)–216.3(3) pm (average value: 211.7 pm). The Sn2 and Sn3 cations coordinate three oxygen atoms and to the fluoride atom. Sn2 coordinates the oxygen atoms O1, O5, and O6 in the range of 209.7(3)–274.6(3) pm (average value: 235.1 pm), and to F1 with an interatomic distance of 206.2(3) pm corresponding to a Sn–F single bond. The Sn3 cation coordinates to the oxygen atoms O1, O2, and O4 with Sn–O distances in the range of 210.7(3) to 244.8(3) pm (average value: 222.1 pm), and to F1 with an interatomic distance of 233.5(3) pm. From Figure 2 it is obvious that all Sn^{2+} cations exhibit a stereochemically active $5s^2$ lone electron pair directed into the open flank of each coordination environment; the O–Sn–X (X=O, F) angles of the closest three neighbours just below 90° (76.2(1)–90.8(1)°) indicate the p character of the bonding interactions. Figure 3a represents the structure of $\text{Sn}_3[\text{B}_3\text{O}_7]\text{F}$ along the *a* axis, where the connections between the Sn, O, and F atoms are shown. Figure 3b shows the connectivity of the three tin atoms with the corresponding oxygen atoms and the unique fluoride atom in enlarged form with the relevant interatomic distances. Sn1 and Sn3 are interconnected via the two oxygen atoms O2 and O4, like in the compound $\text{Sn}_2\text{B}_3\text{O}_6(\text{OH})$.^[20] The Sn–O distances are in the range of 209.2(3) to 244.8(3) pm.

The charge distribution of the atoms in the compound $\text{Sn}_3[\text{B}_3\text{O}_7]\text{F}$ was calculated according to the BLBS (bond-length/bond-strength, ΣV)^[24–28] and the CHARDI (charge distribution in solids) concept (ΣQ). The results are listed in Table S3 given in the Supporting Information, and are consistent with the formal valence states of the cations and anions.

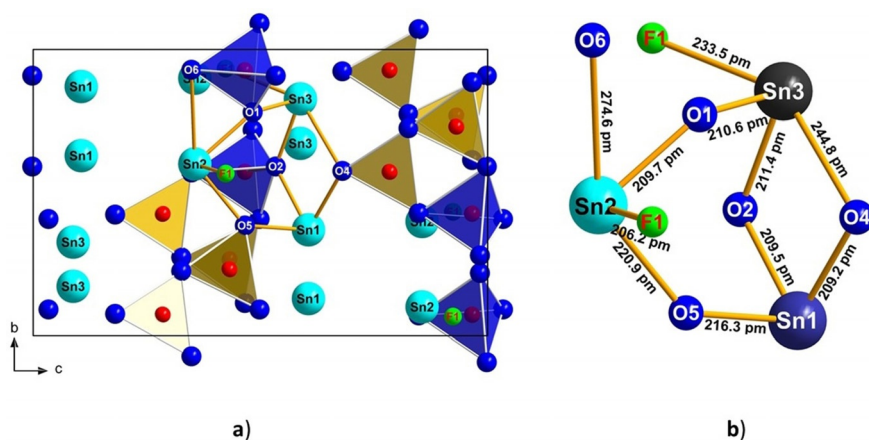


Figure 3. a) The unit cell of $\text{Sn}_3[\text{B}_3\text{O}_7]\text{F}$ along the *a* axis. In the centre of Figure 3a, the coordination between the Sn^{2+} cations (light blue spheres), the O^{2-} atoms (dark blue spheres), and the F^- anions (yellow spheres) are presented; b) Enlarged representation of the coordination between the Sn, O, and F atoms, with the corresponding interatomic distances.

Vibrational spectroscopy

Figure 4 shows the experimental IR and Raman spectra recorded from powder samples, in comparison to the results of density functional theory-based calculations. An extended IR spectrum (4000 to 400 cm^{-1}) is shown in Figure S1 in the Supporting Information. Above 1600 cm^{-1} no bands were recorded,

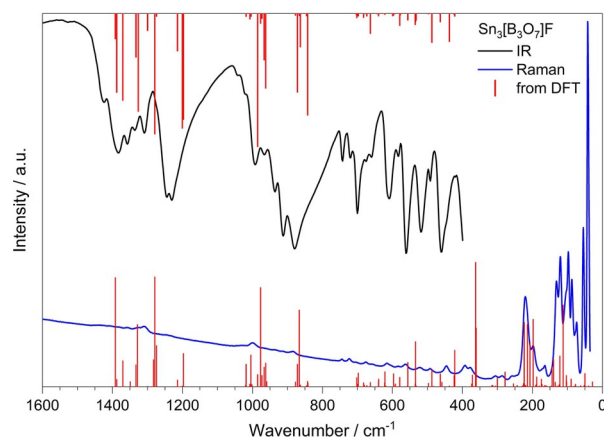


Figure 4. IR (black) and Raman (blue) spectra of $\text{Sn}_3[\text{B}_3\text{O}_7]\text{F}$. The red bars denote band positions calculated by DFT.

which is a very strong indication for the absence of hydroxyl groups. The existence of triangular BO_3 and tetrahedral BO_4 groups in the structure was confirmed. The strong bands between 1600 and 800 cm^{-1} are typical B–O stretching vibrations, whereby the bands of $[\text{BO}_3]^{3-}$ vibrations are expected between 1450 and 1150 cm^{-1} ,^[29–31] and the absorption peaks of the asymmetric and symmetric stretching modes of the BO_4 groups are located in the range between 1050 and 800 cm^{-1} .^[30–32] The bands between 800 and 400 cm^{-1} can be assigned to bending vibrations of BO_3 and BO_4 groups,^[33] as well as ring breathing modes. The experimental Raman spectrum suffers from very low intensities above 250 cm^{-1} and allows only the determination of the frequencies of lattice vi-

brations in the range 250 to 35 cm⁻¹. According to group theory, the irreducible representations of Sn₃[B₃O₇]F are 42A₁ + 42A₂ + 42B₁ + 42B₂. The three acoustic modes have the irreducible representations A₁ + B₁ + B₂. All optical modes (Γ_{Raman} = 41A₁ + 42A₂ + 41B₁ + 41B₂) are Raman active. The infrared active modes have representations Γ_{IR} = 41A₁ + 41B₁ + 41B₂ and all A₂ modes are infrared inactive.

UV/Vis-NIR spectroscopy

Figure 5a illustrates the UV/Vis-NIR diffuse-reflectance spectrum of Sn₃[B₃O₇]F. Apparently, the cut off edge is lower than 263 nm, potentially making Sn₃[B₃O₇]F suitable for UV NLO applications. Based on the UV/Vis-NIR diffuse-reflectance spectrum, the absorption (*K/S*) data were calculated from the Kubelka–Munk function [Eq. (1)]:^[34–36]

$$F(R) = \frac{(1 - R)^2}{2R} = \frac{K}{S} \quad (1)$$

where *R* is the reflectance, *K* the absorption, and *S* is the scattering. Furthermore, the experimental band gap of 4.30 eV is shown in Figure 5b.

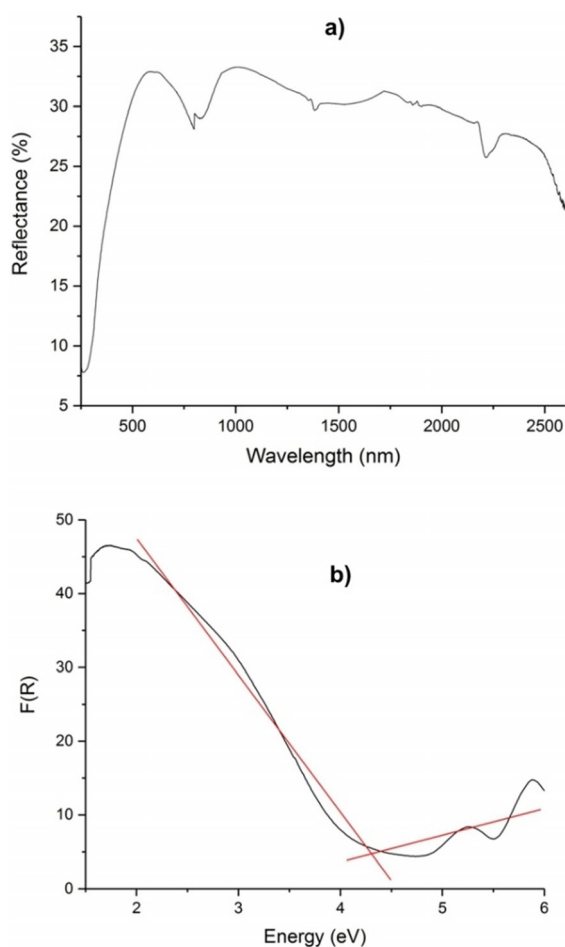


Figure 5. a) UV/Vis-NIR diffuse-reflectance spectrum of Sn₃[B₃O₇]F; b) The UV/Vis-NIR absorption spectrum calculated from the reflectance spectrum for Sn₃[B₃O₇]F.

Thermal behaviour

To study the high-temperature stability of Sn₃[B₃O₇]F, thermo-analytical measurements were performed. Figure 6 illustrates the results from differential scanning calorimetry (DSC) and thermogravimetric analysis (TG), which were recorded from ambient temperature to 550 °C and 1000 °C, respectively.

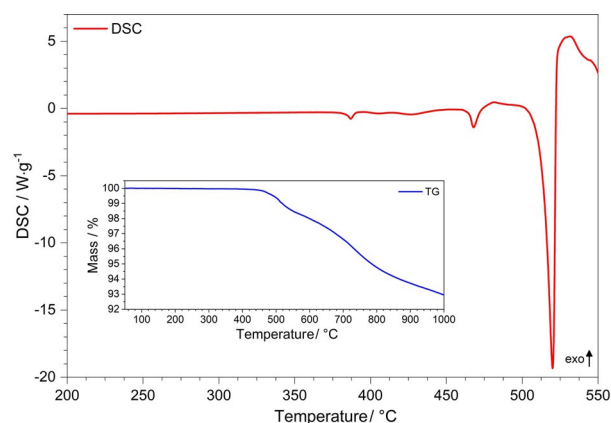


Figure 6. The simultaneous thermal analysis (STA) of Sn₃[B₃O₇]F with the thermogravimetric curve (TG) in blue and the differential scanning calorimetry curve (DSC) in red.

Sn₃[B₃O₇]F is stable up to a temperature of 490 °C. There are three endothermic peaks in the investigated range. The first one, with an onset temperature of 380 °C, is probably due to the conversion of a small amount of Sn[B₂O₃F₂] contaminant with concentrations below the detection limit of the powder XRD.^[19] The second peak, with an onset temperature of 465 °C, can be related to the melting point of the small amorphous boron oxide contamination which is also not detectable by powder XRD. The following thermal decomposition of Sn₃[B₃O₇]F is an endothermic one-step process with an onset temperature of 500 °C. The resulting decomposition product is currently still under investigation. The TG curve features at least two decomposition steps, which are poorly resolved. The onset temperature is 450 °C and the continuous mass loss is not finished at 1000 °C. Most probably this is due to the slow evaporation of B₂O₃, but this is still under investigation. In addition, thermoanalytical measurements were performed on a sample of Sn₃[B₃O₇]F with Sn[B₂O₃F₂] as an impurity (see Figure S2 in Supporting Information), showing a slightly different thermal behaviour (due to the mixture): already at 400 °C, a large endothermic maximum could be found, which was accompanied by a mass loss of 5.4%, matching quite well with the calculated mass loss for BF₃ (calculated: 4.4%). Furthermore, HT-PXRD data were collected on this sample revealing the decomposition of Sn₃[B₃O₇]F (containing Sn[B₂O₃F₂] as an impurity) to SnO₂ and a glassy, amorphous phase, which was indicated by the small halo at middle theta angles (see Figure S3). Attempts to isolate and crystallize an intermediate product of the thermal decomposition were not successful.

Second harmonic generation measurements

The SHG measurements were performed on an ungraded powder of $\text{Sn}_3[\text{B}_3\text{O}_7]\text{F}$ employing the powder SHG method,^[37] which is commonly used in the first step to estimate the non-linear optical properties of new SHG materials. The SHG intensity of $\text{Sn}_3[\text{B}_3\text{O}_7]\text{F}$ was 5080(1066) counts and these second-harmonic signal is found to be ≈ 12 times that of quartz and ≈ 0.4 times that of KH_2PO_4 (KDP). This strong SHG signal implies that the sample has large SHG coefficients or is phase matchable. The centrosymmetric reference sample Al_2O_3 shows a SHG intensity of 4(10) counts. Table 1 illustrates the intensities of the $\text{Sn}_3[\text{B}_3\text{O}_7]\text{F}$ sample and all three reference materials. The point group $mm2$ has five independent SHG coefficients (d_{31} , d_{32} , d_{33} , d_{15} , and d_{24}).

Table 1. SHG intensities of the $\text{Sn}_3[\text{B}_3\text{O}_7]\text{F}$ sample compared with the three reference materials.

Samples	SHG intensity in counts
Al_2O_3	4(10)
Quartz	420(54)
$\text{Sn}_3[\text{B}_3\text{O}_7]\text{F}$	5080(1066)
KDP (KH_2PO_4)	12953(1512)

DFT calculation

Quantum chemical calculations in the framework of density functional theory (DFT) were performed to investigate the electronic structure of $\text{Sn}_3[\text{B}_3\text{O}_7]\text{F}$, in order to interpret the experimentally determined vibrational spectra. The obtained vibrational frequencies are in very good agreement with the experimental values as shown in Figure 4 and discussed above. The lattice parameters obtained by full geometry optimisations are slightly overestimated as a consequence of the PBE exchange-correlation functional employed here with $a=954$, $b=772$, and $c=1222$ pm. In this context, it should be mentioned that DFT-PBE usually overestimates lattice parameters and underestimates optical band gaps.

From electronic band structure calculations, an indirect band gap of 3.8 eV, which underestimates the experimental optical band gap of 4.3 eV, is obtained. This is a common and well-known effect of the standard functionals in DFT. Further, partial densities of states (PDOS) point out that the valence band mainly consists of Sn 5s, Sn 5p, and O 2p orbitals, whereas the conduction band is almost exclusively formed from Sn 5p contributions (see Figure S5).

Real space bonding analysis through the electron localization function (ELF) was carried out to visualize covalent bonds and lone pairs of the title compound. High values of the ELF (0.85) appear in regions of the covalent B–O bonds and further highlight the stereochemically active lone pairs of the Sn^{2+} cations, as well as the lone pairs of the O and F atoms (Figure 7).

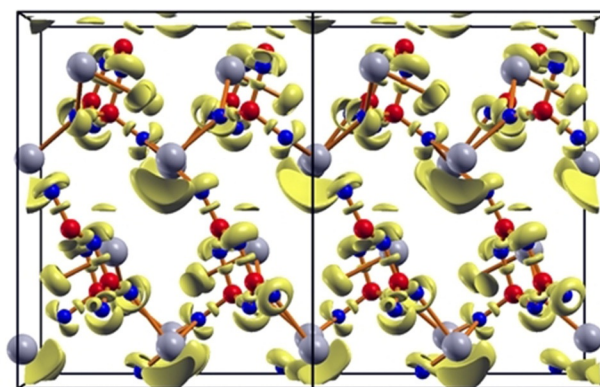


Figure 7. Electron localization function (ELF) (isosurface at 0.85) showing the attractors of the B–O bonds, O lone pairs, F lone pairs, and structure directing lone pairs of Sn^{2+} . Colour code: Isosurface (yellow), boron (red), oxygen (blue), tin (grey); the fluorine atoms are not visible due to the overlapping ELF isosurface.

Conclusion

$\text{Sn}_3[\text{B}_3\text{O}_7]\text{F}$ is the first compound in the system Sn–B–O–F, which was synthesized by a straightforward, cost-efficient hydrothermal synthesis. The structure contains isolated B_3O_7 rings. Between layers of these isolated three membered rings, the Sn1 and Sn3 cations are alternatingly ordered. The Sn2 cations and the F anions are located in a row with the B_3O_7 units.

Experimental Section

Synthesis

$\text{Sn}_3[\text{B}_3\text{O}_7]\text{F}$ was synthesized hydrothermally in a stainless-steel autoclave (volume: 8 mL) with a Teflon insert. A mixture of SnO [107 mg, 0.8 mmol, Strem Chemicals, Inc. ($\geq 99.8\%$, Newburyport, USA)], SnF_2 [78 mg, 0.5 mmol, p.a., Alfa Aesar (Karlsruhe, Germany)], and H_3BO_3 [119 mg, 1.9 mmol, Roth GmbH + Co. KG ($\geq 99.8\%$, Karlsruhe, Germany)] was heated up to a temperature of 510 K and kept there for 4 days. Afterwards, the reaction mixture was cooled down with a rate of two degrees per hour down to 330 K and finally quenched to room temperature. A light greyish powder was obtained and analysed by X-ray powder diffraction. Furthermore, transparent, colourless platelets of $\text{Sn}_3[\text{B}_3\text{O}_7]\text{F}$ were isolated and measured by single-crystal X-ray diffraction. Via this route, the compound $\text{Sn}_3[\text{B}_3\text{O}_7]\text{F}$ could be synthesized with only a minor contamination by $\text{Sn}[\text{B}_2\text{O}_3\text{F}_2]$. According to Figure 8, a phase pure product could be obtained via an alternate synthesis starting from $\text{Sn}[\text{B}_2\text{O}_3\text{F}_2]$,^[19] which decomposes around 400 °C yielding the title compound in the form of large single-crystals. This is consistent with the results of HT-XRD (Figure S3 in Supporting Information), which show that the reflections of the impurity phase $\text{Sn}[\text{B}_2\text{O}_3\text{F}_2]$ vanish at 400 °C.

Crystal structure analysis

The product $\text{Sn}_3[\text{B}_3\text{O}_7]\text{F}$ was identified by powder X-ray diffraction data collected with a Seifert XRD T/T 3003 powder diffractometer in reflection geometry with $\text{Cu}_{K\alpha}$ ($\lambda = 154.056$ pm) radiation, equipped with a Meteor 1D linear detector. Figure 8 shows the experimental powder pattern of $\text{Sn}_3[\text{B}_3\text{O}_7]\text{F}$ at the top compared to

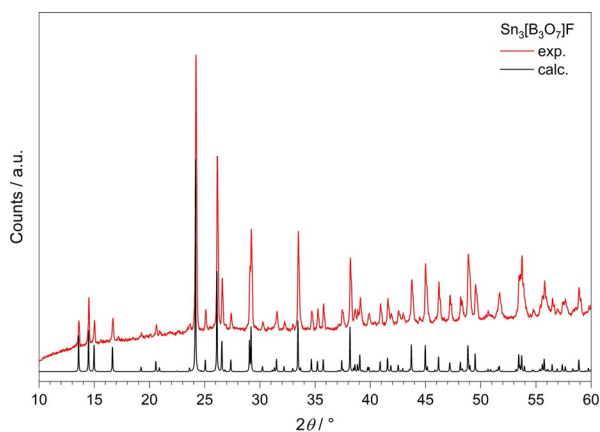


Figure 8. Experimental powder pattern (Cu α radiation; $\lambda = 154.056$ pm) (top), compared with the calculated powder pattern of Sn $_3$ [B $_3$ O $_7$]F (bottom).

the theoretical pattern derived from the single-crystal data. For the single-crystal structure analysis, a colourless platelet of Sn $_3$ [B $_3$ O $_7$]F was isolated through polarization contrast microscopy and analysed via single-crystal X-ray diffraction. The intensity data were collected at 180 K with a Bruker D8 Quest diffractometer (Photon 100) equipped with an Incoatec Microfocus source generator (multi layered optics monochromatized Mo α radiation, $\lambda = 71.073$ pm). Multi-scan absorption corrections were applied with the program SADABS-2014/5.^[38]

After structure solution and parameter refinement with anisotropic displacement parameters for all atoms using the SHELXS/L-13 software suite,^[39,40] the space group *Pna*2 $_1$ was found to be correct. All

Table 2. Crystal data and structure refinement of Sn $_3$ [B $_3$ O $_7$]F (standard deviations in parentheses).

empirical formula	Sn $_3$ B $_3$ O $_7$ F
molar mass [g mol $^{-1}$]	519.5
crystal system	orthorhombic
space group	<i>Pna</i> 2 $_1$ (no. 33)
single-crystal diffractometer	Bruker D8 QUEST PHOTON 100
radiation; wavelength [pm]	Mo α ; $\lambda = 71.073$
<i>a</i> [pm]	922.38(4)
<i>b</i> [pm]	769.78(4)
<i>c</i> [pm]	1221.88(6)
<i>V</i> [nm 3]	867(7)
formula units per cell, <i>Z</i>	4
calculated density [g cm $^{-3}$]	3.977
crystal size [mm]	0.055 × 0.035 × 0.015
temperature [K]	183(2)
absorption coefficient [mm $^{-1}$]	8.59
<i>F</i> (000) [e]	920
2θ range [deg]	6.26–70.01
range in <i>hkl</i>	–14 ≤ <i>h</i> ≤ 14 –12 ≤ <i>k</i> ≤ 12 –19 ≤ <i>l</i> ≤ 19
total no. of reflections	24503
independent reflections/ <i>R</i> $_{int}$	3820/0.0364
reflections with <i>I</i> > 2 σ (<i>I</i>)	24503
data/refined parameters	3820/127
absorption correction	multi-scan (Bruker SADABS 2014/5)
goodness-of-fit on <i>F</i> $_o^2$	1.072
final <i>R</i> 1/ <i>wR</i> 2 [<i>I</i> > 2 σ (<i>I</i>)]	0.0217/0.0399
<i>R</i> 1/ <i>wR</i> 2 (all data)	0.0256/0.0407
Flack parameter	0.016(1)

atoms were refined with anisotropic displacement parameters. All relevant details of the data collections and evaluations are shown in the Tables 2, Table 3, and Table 4. Tables S1 and S2 given in the Supporting Information show the positional parameters and the anisotropic displacement parameters, respectively. Further details of the crystal structure investigation(s) may be obtained from Fachinformationszentrum Karlsruhe, 76344 Eggenstein-Leopoldshafen, Germany (fax: (+49)7247-808-666; e-mail: crysdata@fiz-karlsruhe.de, <https://www.fiz-karlsruhe.de/en/leistungen/kristallographie/kristallstrukturdepot/order-form-request-for-deposited-data.html>) on quoting the deposition number CSD-434719.

Table 3. Selected interatomic distances [pm] in Sn $_3$ [B $_3$ O $_7$]F (standard deviations in parentheses).

Sn1-O2	209.5(3)	B1-O3	135.1(5)
Sn1-O4	209.2(3)	B1-O5	137.4(5)
Sn1-O5	216.3(3)	B1-O7	138.2(5)
	$\emptyset = 211.7$		$\emptyset = 136.7$
Sn2-O1	209.7(3)	B2-O1 ^[1]	147.2(5)
Sn2-O5	221.0(3)	B2-O2	145.9(5)
Sn2-O6	274.6(3)	B2-O3 ^[5]	148.1(5)
Sn2-F1	206.2(3)	B2-O6 ^[5]	148.8(6)
	$\emptyset = 227.7$		$\emptyset = 147.5$
Sn3-O1	210.7(3)	B3-O4 ^[6]	136.0(6)
Sn3-O2	211.4(3)	B3-O6	135.8(5)
Sn3-O4	244.8(3)	B3-O7	138.4(5)
Sn3-F1 ^[1]	233.5(3)		$\emptyset = 136.7$
	$\emptyset = 225.1$	F1-Sn2	206.2(3)
		F1-Sn3 ^[2]	233.5(3)
			$\emptyset = 219.9$

^[1] $1/2 + x, 3/2 - y, + z$; ^[2] $1/2 + x, 3/2 - y, + z$; ^[3] $1/2 + x, 1/2 - y, + z$; ^[4] $1/2 - x, 1/2 + y, 1/2 + z$; ^[5] $1/2 + x, 1/2 - y, + z$; ^[6] $1/2 - x, -1/2 + y, -1/2 + z$.

Table 4. Bond angles [°] for Sn $_3$ [B $_3$ O $_7$]F (standard deviations in parentheses).

O2-Sn1-O5	82.5(1)	O3-B1-O5	121.2(4)
O4-Sn1-O2	76.2(1)	O3-B1-O7	121.6(4)
O4-Sn1-O5	90.5(1)	O5-B1-O7	117.1(4)
	$\emptyset = 83.1$		$\emptyset = 120.0$
O1-Sn2-O5	90.8(1)	O1 ^[1] -B2-O3 ^[5]	109.7(3)
F1-Sn2-O1	83.7(1)	O1 ^[1] -B2-O6 ^[5]	108.0(3)
F1-Sn2-O5	84.1(1)	O2-B2-O1 ^[1]	111.0(3)
	$\emptyset = 86.2$	O2-B2-O3 ^[5]	107.1(3)
		O2-B2-O6 ^[5]	109.8(3)
O1-Sn3-O2	88.8(1)	O3-B2-O6 ^[5]	111.2(3)
O1-Sn3-O4	80.3(1)		$\emptyset = 109.5$
O1-Sn3-F1 ^[1]	79.8(1)		
O2-Sn3-O4	68.5(1)	O4 ^[6] -B3-O7	117.5(4)
O2-Sn3-F1 ^[1]	83.0(1)	O6-B3-O4 ^[6]	122.3(4)
F1 ^[1] -Sn3-O4	145.3(1)	O6-B3-O7	120.2(4)
	$\emptyset = 91.0$		$\emptyset = 120.0$

^[1] $1/2 + x, 3/2 - y, + z$; ^[2] $1/2 + x, 3/2 - y, + z$; ^[3] $1/2 + x, 1/2 - y, + z$; ^[4] $1/2 - x, 1/2 + y, 1/2 + z$; ^[5] $1/2 + x, 1/2 - y, + z$; ^[6] $1/2 - x, -1/2 + y, -1/2 + z$.

Vibrational spectroscopy

An FTIR-ATR (Attenuated Total Reflection) characterization of the Sn $_3$ [B $_3$ O $_7$]F powder sample was performed in the spectral range of 400–4000 cm $^{-1}$ with a Bruker ALPHA Platinum-ATR spectrometer

(Bruker, Billerica, USA) equipped with a 2×2 mm diamond ATR-crystal and a DTGS detector. 320 scans of the powder sample were acquired and afterwards corrected for atmospheric influences using the Opus 7.2 software.^[41]

Raman spectroscopy

Raman spectra were recorded on a Thermo Scientific DXR Raman-Microscope in the range 1800–60 cm⁻¹ using a 532 nm laser operated with 10 mW power. The sample was illuminated for 3600 s (10-fold magnification, 50 μm pinhole aperture, high resolution grating (1800 lines mm⁻¹), spectral resolution 1 cm⁻¹).

UV/Vis-NIR spectroscopy

The UV/Vis diffuse reflection data were recorded at ambient temperature. A powder sample of BaSO₄ has been used as standard (100% reflectance). The spectrum of the Sn₃[B₃O₇]F powder was recorded from 190 to 2600 nm using an Agilent Cary 5000 UV/Vis-NIR spectrophotometer at ambient temperature.

Thermoanalytical investigation

The TG curve (Figure 7) was recorded on a TA Instrument Q500 TGA in a 90 mL min⁻¹ nitrogen flow using an Al₂O₃ crucible; the DSC measurement was undertaken on a TA Instrument DSC 2920 in a 50 mL min⁻¹ nitrogen flow using a Netzsch standard Al pan with pierced lid. Both measurements were performed with heating rates of 5 °C min⁻¹.

High temperature XRD

The high temperature X-ray diffraction patterns were obtained on an Empyrean powder diffractometer (Panalytical) in theta-theta geometry, equipped with a Cu tube with 40 kV tube tension and 40 mA tube current, and a Pixcel 1D detector. Furthermore, a variable divergence slit was used with an irradiated length of 6 mm. The sample was applied to the platinum strip (thickness of the platinum strip: 1 mm) and measured in an Anton Paar HTK 16N high temperature strip-heater chamber under air and in a temperature range from 300 K to 870 K.

Second harmonic generation measurements

According to the non-centrosymmetric orthorhombic space group *Pna*₂₁ (no. 33), the SHG effect of the Sn₃B₃O₇F compound was tested. A detailed description of the experimental setup for the powder SHG measurement is given by Bayarjargal et al.^[42] The SHG measurement was performed on a Q-switched Nd:YLF laser system (Falcon 217D, Quantronix) operating at 1054 nm and with a pulse width of 130 ns, which provided the fundamental wave. The sample was placed on an adhesive tape, which did not generate a SHG signal. The SHG signal was detected at 527 nm. From five different areas of the sample, SHG measurements were performed with 15 measurements at each position, and the intensities of these five different positions were averaged, to check the homogeneity of the sample. The measured intensities were collected by subtracting a background signal, which was collected between the pulses. As reference materials, quartz (α-SiO₂), Al₂O₃, and KDP powders were used.

DFT calculations

Quantum chemical calculations were performed in the framework of density functional theory (DFT) using a linear combination of

Gaussian-type functions (LCGTF) scheme as implemented in CRYSTAL14.^[43,44] The total energy calculations including full structural optimizations were performed with the GGA (PBE)^[45] xc-functional. The convergence criterion considering the energy was set to 1×10 a.u. with a k-mesh sampling of 6×6×6. All-electron basis sets were taken from references [46–48] and the outermost coefficients of the contractions were optimised. The vibrational frequencies, including Raman intensities, were computed on the basis of the relaxed structures using the coupled-perturbed Kohn–Sham (CPKS) mode.^[49,50] Vibrational modes were visualized with the J-ICE application.^[51] The electronic structure was additionally assessed by the full potential local orbital (FPLO) method as implemented in the FPLO code (version 14.00–45).^[52] Scalar-relativistic PBE calculations were carried out on a k-mesh of 4×4×4. Further, a direct space analysis of the charge density was carried out by calculating the electron localization function (ELF) with TOPOND^[53] interfaced to CRYSTAL14. 3D plots were visualized with XCrysDen.^[54]

Acknowledgements

We thank Dr. K. Wurst and Dr. G. Heymann for collecting the single-crystal data and we are very thankful to the Institute for Construction and Materials Science at the University of Innsbruck for granting us access to the devices for the thermoanalytical measurements. F.P. thanks the Computer Service Group at the Max-Planck-Institute for Solid State Research (Stuttgart, Germany) for providing computational facilities. H.A.H. and S.G.J. thank Hannes Radinger (Universität Augsburg) for valuable assistance during preliminary work on the topic of borate fluorides.

Conflict of interest

The authors declare no conflict of interest.

Keywords: borate • hydrothermal synthesis • SHG measurements • structure elucidation • thermoanalytical measurements • tin fluoride borate

- [1] P. A. Franken, A. E. Hill, C. W. Peters, G. Weinreich, *Phys. Rev. Lett.* **1961**, *7*, 118–119.
- [2] G. Zou, C. Lin, H. Jo, G. Nam, T.-S. You, K. M. Ok, *Angew. Chem. Int. Ed.* **2016**, *55*, 12078–12082; *Angew. Chem.* **2016**, *128*, 12257–12261.
- [3] P. Becker, *Adv. Mater.* **1998**, *10*, 979–992.
- [4] Z. Lin, X. Jiang, L. Kang, P. Gong, S. Luo, M.-H. Lee, *J. Phys. D: Appl. Phys.* **2014**, *47*, 253001.
- [5] C. T. Chen, Y. C. Wu, A. D. Jiang, G. M. You, *Sci. Sin., Ser. B (Engl. Ed.)* **1985**, *28*, 235–243.
- [6] S.-i. Furusawa, O. Chikagawa, S. Tange, T. Ishidate, H. Orihara, Y. Ishibashi, K. Miwa, *J. Phys. Soc. Jpn.* **1991**, *60*, 2691–2693.
- [7] Y. Wu, T. Sasaki, S. Nakai, A. Yokotani, H. Tang, C. Chen, *Appl. Phys. Lett.* **1993**, *62*, 2614–2615.
- [8] J.-M. Tu, D. A. Keszler, *Mater. Res. Bull.* **1995**, *30*, 209–215.
- [9] Y. Mori, I. Kuroda, S. Nakajima, T. Sasaki, S. Nakai, *Appl. Phys. Lett.* **1995**, *67*, 1818–1820.
- [10] M. Iwai, T. Kobayashi, H. Furuya, Y. Mori, T. Sasaki, *Jpn. J. Appl. Phys.* **1997**, *36*, L276.
- [11] L. Mei, Y. Wang, C. Chen, B. Wu, *J. Appl. Phys.* **1993**, *74*, 7014–7015.
- [12] H. Li, H. Wu, X. Su, H. Yu, S. Pan, Z. Yang, Y. Lu, J. Han, K. R. Poeppelmeier, *J. Mater. Chem. C* **2014**, *2*, 1704–1710.
- [13] H. Yu, H. Wu, S. Pan, Z. Yang, X. Su, F. Zhang, *J. Mater. Chem.* **2012**, *22*, 9665–9670.

- [14] G. Zou, L. Zhang, N. Ye, *CrystEngComm* **2013**, *15*, 2422–2427.
- [15] R. Cong, Y. Wang, L. Kang, Z. Zhou, Z. Lin, T. Yang, *Inorg. Chem. Front.* **2015**, *2*, 170–176.
- [16] Z. Zhang, Y. Wang, B. Zhang, Z. Yang, S. Pan, *Angew. Chem. Int. Ed.* **2018**, *57*, 6577–6581; *Angew. Chem.* **2018**, *130*, 6687–6691.
- [17] M. Mutailipu, M. Zhang, B. Zhang, L. Wang, Z. Yang, X. Zhou, S. Pan, *Angew. Chem. Int. Ed.* **2018**, *57*, 6095–6099; *Angew. Chem.* **2018**, *130*, 6203–6207.
- [18] X. Wang, Y. Wang, B. Zhang, F. Zhang, Z. Yang, S. Pan, *Angew. Chem. Int. Ed.* **2017**, *56*, 14119–14123; *Angew. Chem.* **2017**, *129*, 14307–14311.
- [19] S. G. Jantz, L. Dialer, L. Bayarjargal, B. Winkler, L. Van Wüllen, F. Pielnhöfer, J. Brgoch, R. Weihrich, H. A. Höpfe, *Adv. Opt. Mater.* **2018**, *6*, 1800497.
- [20] S. Schöneegger, K. Wurst, G. Heymann, A. Schaur, A. Saxer, D. Johrendt, H. Huppertz, *J. Solid State Chem.* **2018**, *258*, 410–415.
- [21] S. Schöneegger, K. Wurst, G. Heymann, A. Schaur, A. Saxer, D. Johrendt, H. Huppertz, *Z. Naturforschung B* **2018**, *73*, 337–348.
- [22] P. C. Burns, J. D. Grice, F. C. Hawthorne, *Can. Mineral.* **1995**, *33*, 1131–1151.
- [23] E. Zobel, *Z. Kristallogr.* **1990**, *191*, 45–57.
- [24] L. Pauling, *J. Am. Chem. Soc.* **1947**, *69*, 542.
- [25] A. Byström, K.-A. Wilhelmi, *Acta Chem. Scand.* **1951**, *5*, 1003.
- [26] I. D. Brown, D. Altermatt, *Acta Crystallogr. Sect. B* **1985**, *41*, 244–247.
- [27] N. E. Brese, M. O. Keeffe, *Acta Crystallogr. Sect. B* **1991**, *47*, 192–197.
- [28] M. O’Keeffe in *Structure and Bonding*, Vol. 71, Springer, Berlin, Heidelberg, **1989**, pp. 162–190.
- [29] R. Hoppe, S. Voigt, H. Glaum, J. Kissel, H. P. Müller, K. J. Bernet, *J. Less-Common Met.* **1989**, *156*, 105–122.
- [30] K. Machida, H. Hata, K. Okuno, G. Adachi, J. Shiokawa, *J. Inorg. Nucl. Chem.* **1979**, *41*, 1425–1430.
- [31] J. P. Laperches, P. Tarte, *Spectrochim. Acta* **1966**, *22*, 1201–1210.
- [32] S. D. Ross, *Spectrochim. Acta* **1972**, *28*, 1555–1561.
- [33] H. R. Xia, L. X. Li, B. Teng, W. Q. Zheng, G. W. Lu, H. D. Jiang, J. Y. Wang, *J. Raman Spectrosc.* **2002**, *33*, 278–282.
- [34] A. B. Murphy, *J. Phys. D: Appl. Phys.* **2006**, *39*, 3571.
- [35] L. Yang, B. Kruse, *J. Opt. Soc. Am. A* **2004**, *21*, 1933–1941.
- [36] J. Tauc, *Mater. Res. Bull.* **1970**, *5*, 721–729.
- [37] S. K. Kurtz, T. T. Perry, *J. Appl. Phys.* **1968**, *39*, 3798.
- [38] Bruker, SADABS, v2014/5, Bruker AXS Inc., Madison, WI, USA **2001**.
- [39] G. M. Sheldrick, SHELXL-2013/1, Program Suite for the Solution and Refinement of Crystal Structures, University of Göttingen (Germany) **2013**.
- [40] G. Sheldrick, *Acta Crystallogr. Sect. C* **2015**, *71*, 3–8.
- [41] Bruker, OPUS v7.2, Bruker, Billerica, USA **2012**.
- [42] L. Bayarjargal, B. Winkler, E. Haussühl, R. Boehler, *Appl. Phys. Lett.* **2009**, *95*, 061907.
- [43] R. Dovesi, V. R. Saunders, C. Roetti, R. Orlando, C. M. Zicovich-Wilson, F. Pascale, B. Civalleri, K. Doll, N. M. Harrison, I. J. Bush, P. D’Arco, M. Llunell, M. Causa, Y. Noel, *CRYSTAL14 User’s Manual*, **2014**.
- [44] R. Dovesi, R. Orlando, A. Erba, C. M. Zicovich-Wilson, B. Civalleri, S. Cassassa, L. Maschio, M. Ferrabine, M. D. L. Pierre, P. D’Arco, Y. Noel, M. Causa, M. Rerat, B. Kirtman, *Int. J. Quantum Chem.* **2014**, *114*, 1287.
- [45] J. P. Perdew, K. Burke, M. Ernzerhof, *Phys. Rev. Lett.* **1996**, *77*, 3865–3868.
- [46] R. Orlando, R. Dovesi, C. Roetti, V. R. Saunders, *J. Phys. Condens. Matter* **1990**, *2*, 7769.
- [47] J. Scaranto, S. Giorgianni, *J. Mol. Struct.* **2008**, *858*, 72–76.
- [48] R. Nada, C. R. A. Catlow, C. Pisani, R. Orlando, *Modell. Simul. Mater. Sci. Eng.* **1993**, *1*, 165.
- [49] M. Ferrero, M. Rérat, R. Orlando, R. Dovesi, *J. Comput. Chem.* **2008**, *29*, 1450–1459.
- [50] M. Ferrero, M. Rérat, B. Kirtman, R. Dovesi, *J. Chem. Phys.* **2008**, *129*, 244110.
- [51] P. Canepa, R. M. Hanson, P. Ugliengo, M. Alfreðsson, *J. Appl. Crystallogr.* **2011**, *44*, 225.
- [52] K. Koepf, H. Eschrig, *Phys. Rev. B* **1999**, *59*, 1743–1757.
- [53] C. Gatti, S. Cassassa, Topond14-<http://www.crystal.unito.it/topond/topond.pdf>, **2016**.
- [54] A. Kokalj, *Comput. Mater. Sci.* **2003**, *28*, 155–168.

 Manuscript received: July 9, 2018

Accepted manuscript online: August 5, 2018

Version of record online: September 5, 2018